Jiang *et al. Biochar* (2026) 8:112
https://doi.org/10.1007/s42773-026-00620-0

Biochar

ORIGINAL RESEARCH Open Access

Nanozeolite-coupled biochar-based phosphate fertilizer dampens warming-induced soil carbon loss by microbial functional constraints in Moso bamboo forests

Zhenhui Jiang[1], Caixian Tang[2], Yunying Fang[3], Tida Ge[4], Shuokang Liu[1], Yu Luo[5], Bing Yu[1], Yanjiang Cai[1], Jason C. White[6] and Yongfu Li[1*]

Abstract

Using nanozeolite-coupled biochar-based phosphate fertilizers (NanoBP) has been proposed as a promising strategy to improve phosphorus-use efficiency in intensive crop systems, yet the effects of NanoBP on soil organic carbon (SOC) mineralization and its temperature sensitivity (Q_{10}) in forests remain poorly understood. In this 56-day incubation study, we examined how NanoBP and conventional chemical phosphorus fertilizer (CP), supplying comparable amounts of phosphorus, influenced SOC mineralization and its apparent Q_{10} in a Moso bamboo forest soil. Compared with the unfertilized control, CP application increased SOC-derived CO_2 emissions but showed little effect on Q_{10}. In contrast, NanoBP lowered SOC mineralization rates and Q_{10} across both active and slow carbon pools. Variations in Q_{10} were primarily driven by microbial enzyme activities and the abundance of cellulolytic functional genes. Despite higher soil microbial biomass and phosphorus availability, NanoBP suppressed β-glucosidase and cellobiohydrolase activities and reduced the abundance of *GH48* and *cbh*I genes. These findings indicate that NanoBP may dampen the Q_{10} through constraining microbial functional traits. The study provides mechanistic insights into SOC mineralization responses under controlled conditions and may inform carbon management strategies in intensively managed bamboo forests, pending field-scale validation.

Highlights

- Conventional phosphate fertilizer increased soil organic carbon (SOC) mineralization.
- Nanozeolite-coupled biochar-based phosphate reduced both SOC mineralization and Q_{10}.
- Active and slow carbon pools exhibited similar Q_{10}.
- Q_{10} was driven by β-glucosidase, cellobiohydrolase, *GH48*, and *cbh*I.

Keywords Biochar-based fertilizer, Enzymatic controls, Functional genes, Q_{10}, Slow carbon pool

*Correspondence:
Yongfu Li
yongfuli@zafu.edu.cn
Full list of author information is available at the end of the article

Springer

Graphical Abstract

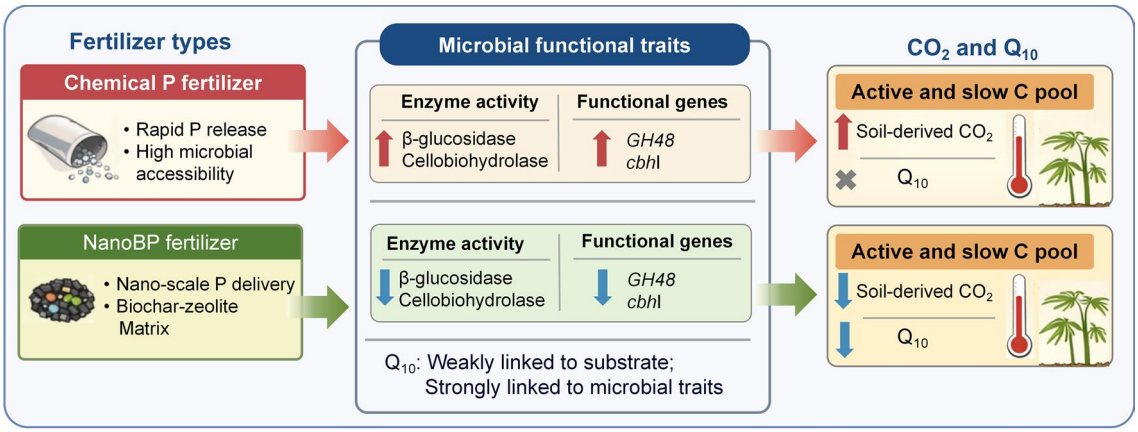

1 Introduction

Soil organic carbon (SOC) constitutes one of the largest carbon (C) pools in terrestrial ecosystems and plays a critical role in regulating climate feedbacks (IPCC 2021). Climate warming is widely recognized to accelerate SOC mineralization, thereby increasing the risk of long-term C loss from soils (Crowther et al. 2016; Sáez-Sandino et al. 2024). These effects are expected to be particularly pronounced in subtropical regions, where high temperature and moisture conditions favor rapid soil organic matter turnover (Liu et al. 2023; Song et al. 2017). Moso bamboo (*Phyllostachys edulis*) forests are a representative subtropical ecosystem that cover more than 4.7 million hectares in southern China and contribute substantially to regional C sequestration because of their high productivity and rapid biomass cycling (Liu et al. 2025; Xiao et al. 2026; Zhou et al. 2024). However, this rapid C cycling may also enhance the temperature sensitivity of SOC mineralization (Q_{10}) and increase its responsiveness to management practices, thereby creating uncertainty about the stability of soil C stocks in intensively managed Moso bamboo systems (Liu et al. 2023; Song et al. 2013).

Conventional phosphorus (CP) fertilizers (e.g., superphosphate) are widely used to sustain the high productivity of bamboo plantations (Islam et al. 2025; Jiang et al. 2025). Highly weathered tropical and subtropical soils are commonly limited by phosphorus (P) deficiency because of strong fixation processes (Duan et al. 2025; Solangi et al. 2023). Although fertilizer inputs can alleviate P limitation and enhance plant growth, fertilization may also stimulate microbial activity and increase C turnover, potentially amplifying SOC mineralization under warming conditions (Zhu et al. 2022; Li et al. 2023). Previous studies have shown that P fertilization can increase Q_{10} (Chen et al. 2022; Zang et al. 2020). Given the potential negative effects of CP on SOC turnover and Q_{10}, alternative fertilizer formulations are needed to better regulate SOC temperature responses in Moso bamboo soils.

Nanozeolite-coupled biochar-based phosphate fertilizer (NanoBP) has recently been proposed as an alternative strategy to improve P-use efficiency (Dong et al. 2025; Li et al. 2025). By integrating nanozeolite, biochar, and phosphate into a composite material, NanoBP differs fundamentally from soluble chemical fertilizers and can regulate P availability through controlled release, spatial distribution, and interactions with soil surfaces (Dong et al. 2025; Feng et al. 2022; Gul et al. 2026; Zhang et al. 2025). These properties may alter soil physicochemical conditions and microbial functional traits, thereby potentially influencing the processes that regulate SOC turnover and Q_{10} (Song et al. 2026; Wu et al. 2025). However, it remains unclear whether such fertilizer formulations modify SOC mineralization and its Q_{10} relative to CP, particularly in bamboo ecosystems exposed to warming.

Understanding these effects requires considering that SOC is composed of multiple pools with contrasting turnover rates that can respond differently to warming (von Lützow et al. 2007; Wu et al. 2026). The mineralization of more stable SOC fractions is often assumed to exhibit higher Q_{10} compared with labile fractions based on kinetic theory (Conant et al. 2011; Knorr et al. 2005). Distinguishing how different SOC pools respond to novel fertilization strategies is therefore essential for improving

predictions of soil C dynamics under global warming (Qin et al. 2019). However, evidence remains scarce regarding how NanoBP influences SOC pool-specific responses in managed bamboo forest soils.

To address this knowledge gap, we conducted an incubation experiment using subtropical bamboo soils to compare the effects of NanoBP and CP supplied at equivalent P levels. The objectives of our study were to (i) quantify their effects on SOC mineralization and Q_{10}, (ii) evaluate whether active and slow SOC pools differ in Q_{10}, and (iii) identify the primary factors associated with observed changes. We tested the following hypotheses. First, SOC mineralization would be higher under CP than under NanoBP because NanoBP provides a more controlled P supply and may limit microbial decomposition processes by modifying nutrient availability. Second, NanoBP would exhibit a lower Q_{10} than CP because its distinct fertilizer properties may impose stronger constraints on microbial C-decomposition processes. Third, fertilization effects on SOC mineralization and Q_{10} would be more pronounced in the slow SOC pool than in the active pool because decomposition of more stable C is more strongly constrained by P availability.

2 Materials and methods

2.1 Soil sampling and fertilizers

The experimental design and soil sampling procedures followed those described in Jiang et al. (2026a). Briefly, topsoil (0–20 cm) was collected from a subtropical Moso bamboo (*Phyllostachys edulis*) stand in Langbi Village, Hangzhou, China (30°13′ N, 119°47′ E). The site has a monsoonal climate and a *Ferralsol* soil (WRB classification). The site had been under intensive management since 2009, when the original evergreen broadleaf forest was converted to a bamboo plantation. Fertilization had been applied annually with urea (200 kg N ha^{-1}), superphosphate (57 kg P ha^{-1}), and potassium chloride (66 kg K ha^{-1}). The sampled bamboo stand covered approximately 1.2 ha. Soil samples were collected within a 100 m × 120 m area to capture within-site spatial heterogeneity. Eight composite samples were obtained, each composed of five soil cores (0–20 cm) collected randomly within a 20 m × 20 m subplot. After visible roots and stones were removed, soils were passed through a 2-mm sieve and stored at 4 °C for less than one month prior to incubation. The soil had the initial properties including an acidic pH (4.9), SOC (18.6 g kg^{-1} soil), $\delta^{13}C$ (–27.4‰), total N (1.82 g kg^{-1} soil), available P (8 mg kg^{-1} soil), available K (88 mg kg^{-1} soil), and a texture comprised of 42% sand, 31% silt, and 27% clay. This low available P indicated P deficiency (≤ 10 mg kg^{-1} soil) in the soil.

Two P types were used: (1) analytical-grade sodium dihydrogen phosphate (NaH_2PO_4) (CP) and (2) NanoBP. The NanoBP was formulated by mixing nano-zeolite with kaolinite, biochar, and NaH_2PO_4 (Dong et al. 2025). The biochar was produced by pyrolyzing maize straw at 500 °C under O_2 limitation, and had a pH of 9.6, a specific surface area of 11.3 m^2 g^{-1}, C 598 g kg^{-1}, $\delta^{13}C$ –15.3‰, N 13 g kg^{-1}, and a cation exchange capacity of 17 cmol kg^{-1}. Fly-ash zeolite and biochar were ball-milled (600 rpm, 6 h) prior to composite formulation. Biochar, NaH_2PO_4, nano-zeolite, and kaolinite were homogenized at a ratio of 15: 25: 50: 10 (w/w). Kaolinite was incorporated as a structural stabilizer and mineral matrix component to enhance granule integrity and regulate P release kinetics. The mixture was moistened to 20–25% water content before granulation to facilitate aggregation and prevent dust formation. The granules were air-dried at 60 °C, sieved to 2–4 mm to ensure uniform particle size, and used for incubation experiments.

The final product of NanoBP was alkaline (pH 9.2) with a P content of 6.8% (w/w), a cation exchange capacity of 39 cmol kg^{-1}, and a specific surface area of 86 m^2 g^{-1}. Based on a 24-h controlled-release assay (Dong et al. 2025), the NanoBP had slower P release than CP (29% vs. 54%). The X-ray diffraction analysis identified $CaSO_4$ and $CaHPO_4{\cdot}2H_2O$ as the main crystalline phases, confirming successful incorporation of phosphate into the composite matrix. X-ray photoelectron spectroscopy spectra showed that P predominantly existed as HPO_4^{2-} and PO_4^{3-}, while Fourier transform infrared spectroscopy further verified the presence of characteristic functional groups associated with the zeolitic and phosphate components. Dynamic Light Scattering analysis indicated an average nano-zeolite particle size of 575 nm (Dong et al. 2025).

2.2 Experimental design

The incubation experiment consisted of three P treatments (control, no fertilizer input; CP; and NanoBP) and temperature regimes (25 °C and 35 °C), with three replicates in a fully randomized design. The incubation temperature of 35 °C was selected to represent a high-end warming scenario for subtropical Moso bamboo forests, where summer soil temperatures can reach that level. It represents an intensified but environmentally plausible warming condition in the region.

For each replicate treatment, 200 g (dry-mass equivalent) of homogenized soil was placed in a 500-mL incubation jar. The soils were adjusted to 55% of water-holding capacity (WHC) and subsequently pre-incubated in the dark at 25 °C for 7 d. Both P fertilizers were added at a rate of 0.1 mg P g^{-1} dry soil and thoroughly mixed with the soil, the addition rate corresponding to approximately 120 kg P ha^{-1} under field conditions (0–10 cm depth). The moisture was readjusted to 60% WHC, and the jars

were sealed during 56-day incubation at the target temperatures. The 56-day incubation period was chosen to capture short-term SOC mineralization dynamics at different temperatures and to support reliable kinetic model fitting, consistent with previous studies assessing Q_{10} (Qin et al. 2019), rather than to evaluate long-term SOC stabilization.

Soil respiration was monitored on days 2, 7, 14, 28, 42, and 56 of the incubation. Soil CO_2 released from the soil was trapped in 10 mL of 0.1 M NaOH and quantified by back-titration with 0.1 M HCl. To determine its isotopic composition, excess $BaCl_2$ solution was added to the remaining NaOH to precipitate dissolved carbonate as $BaCO_3$, after which the ^{13}C abundance was analyzed using an isotope ratio mass spectrometer (Sercon Hydra 20–22 IRMS, Crewe, Cheshire, UK). At the end of the incubation (day 56), destructive sampling was performed to measure soil pH, available P, microbial biomass C (MBC), water-extractable organic C (WEOC), and activities of extracellular enzymes including β-glucosidase (BG), cellobiohydrolase (CBH), acid phosphatase (AP), and polyphenol oxidase (PO). The abundance and community composition of the cellulolytic genes *cbh*I and *GH48* were also determined.

2.3 Soil-derived CO_2

To trace the sources of soil-derived CO_2 in the NanoBP treatments, the natural $\delta^{13}C$ abundance technique was applied. The biochar derived from maize straw (C_4, $\delta^{13}C = -15.3‰$) differed isotopically from the bamboo soil (C_3, $\delta^{13}C = -27.4‰$), which allowed for the partitioning of CO_2 emissions between the added biochar within the NanoBP and native SOC. Preliminary tests confirmed that the $\delta^{13}C$ values of the biochar (–15.3‰) and native soil (–27.4‰) remained stable throughout the 56-day incubation (variation < 0.2‰). These values were therefore treated as constant end-members in the two-source isotopic mixing model as follows.

$$f_{\mathrm{SOM}} = \frac{\delta^{13}C_{\mathrm{total}} - \delta^{13}C_{\mathrm{biochar}}}{\delta^{13}C_{\mathrm{SOM}} - \delta^{13}C_{\mathrm{biochar}}} \quad (1)$$

$$C_{\mathrm{SOM}} = C_{\mathrm{total}} \times f_{\mathrm{SOM}} \quad (2)$$

where f_{SOM} indicates the fraction of CO_2 derived from soil organic matter (C_{SOM}) relative to the total CO_2 (C_{total}) under NanoBP treatments; $\delta^{13}C_{total}$ refers to the isotopic signature of the total CO_2 emitted from the soil; $\delta^{13}C_{biochar}$ represents the isotopic composition of biochar-derived C; and $\delta^{13}C_{SOM}$ denotes the isotopic signature of soil-derived CO_2, which was determined using CO_2 from the control treatment.

2.4 Calculation of temperature sensitivity

The apparent temperature sensitivity of soil C mineralization was expressed as Q_{10}, calculated as the ratio of cumulative soil-derived CO_2 emissions measured at 35 °C ($T_{35°C}$) to those at 25 °C ($T_{25°C}$).

$$Q_{10} = \left(\frac{Soil - derived\ CO_{2-35°C}}{Soil - derived\ CO_{2-25°C}}\right)^{\frac{10}{T_{35°C} - T_{25°C}}} \quad (3)$$

2.5 Estimation of CO_2 emission rates using single- and double-exponential models

To quantify the potential SOC mineralization rate, temporally cumulative CO_2 emissions were initially fitted using a first-order kinetic one-compartment model:

$$C(t) = C_0 \times \left(1 - e^{-kt}\right) \quad (4)$$

where $C(t)$ is the cumulative CO_2 emission at time t (days); C_0 is the potentially mineralizable C pool (termed "bulk soil, μg C g^{-1} soil); k is the first-order rate constant (day^{-1}), and e is the base of the natural logarithm.

The distinction between active and stable C pools followed the kinetic definition widely used in SOC mineralization models, where the active pool represents the rapidly decomposable substrate and the stable pool represents a relatively slower-turnover component under the incubation conditions (Liang et al. 2015). This approach has been validated in incubation studies of soils and provides a robust means to estimate pool-specific Q_{10} (Qin et al. 2019). To identify whether the active and stable C pools differed in CO_2 release under P amendments, the cumulative CO_2 emissions were also fitted using a two-pool model:

$$C(t) = C_1 \times \left(1 - e^{-k_1 t}\right) + C_2 \times \left(1 - e^{-k_2 t}\right) \quad (5)$$

where C_1 and C_2 are the magnitudes of CO_2 emissions from the active and stable C pools (μg C g^{-1} soil), respectively, and k_1 and k_2 are their corresponding first-order decomposition rate constants (day^{-1}). The model parameters (C_1, C_2, k_1, k_2) were estimated by nonlinear regression using the least-squares method, while the model performance was assessed based on the coefficient of determination (R^2) and the associated significance level (P-value).

Notably, the active and slow C pools estimated from the double-exponential model represent operational kinetic pools defined by fitted turnover rate constants rather than physically isolated SOC fractions. These pools reflect differences in apparent decomposition rates under incubation conditions and should not be directly

interpreted as discrete physicochemical C fractions in soil.

2.6 Determination of soil physicochemical properties

Soil pH was measured with a potentiometer using a soil–water suspension prepared at a ratio of 1:2.5 (w/v). Available P was extracted with a mixture of 0.03 M NH_4F and 0.025 M HCl following the Bray–Kurtz method (Bray and Kurtz 1945), and the extract was then analyzed by colorimetry. For WEOC, 20 g of freshly sieved soil (2 mm) was extracted in deionized water at a 1:2 (w/v) ratio and shaken at 120 rpm for 30 min at 25 °C. The suspension was subsequently centrifuged at 4,000 rpm for 20 min, after which the supernatant was filtered through a 0.45-μm membrane. A 5-mL portion of the filtrate was diluted to 50 mL, and organic C was quantified using a TOC analyzer (TOC-L CSH/CPN, Shimadzu, Kyoto, Japan).

Soil MBC was quantified using the chloroform fumigation–extraction approach (Vance et al. 1987). Briefly, fresh soil (10 g) was divided into two subsamples. One subsample was exposed to ethanol-free chloroform vapor in a sealed vacuum desiccator for 24 h in darkness, whereas the other remained unfumigated as a reference. Following fumigation, both soil portions were extracted with 0.5 M K_2SO_4 (50 mL) by shaking for 30 min at 25 °C. The resulting suspensions were centrifuged at 3,000 rpm for 20 min, and the supernatants were passed through 0.45-μm membrane filters. A 5-mL aliquot of each filtrate was diluted to 50 mL prior to determining dissolved organic C. The MBC was estimated from the difference in extractable C between fumigated and non-fumigated samples, applying a conversion coefficient of 0.45 (Joergensen 1996).

2.7 Analysis of substrate quality

To evaluate the chemical characteristics of SOC as an indicator of substrate quality, the molecular structure of SOC was analyzed using solid-state ^{13}C nuclear magnetic resonance (^{13}C NMR) spectroscopy following the approach of Li et al. (2017). Prior to analysis, soil samples were treated with hydrofluoric acid (HF) to remove mineral components and enrich the organic fraction. The pretreated samples were then subjected to ^{13}C NMR measurement, and the resulting spectra were integrated over defined chemical shift regions. Four major SOC functional groups were quantified based on their chemical shift ranges: alkyl C (0–46 ppm), O-alkyl C (46–114 ppm), aromatic C (114–164 ppm), and carbonyl C (164–220 ppm).

2.8 Determination of soil enzyme activities

The activities of key soil enzymes, including BG, CBH, AP, and PO, were determined to assess their microbial functional potential. All measurements were performed on fresh soil, and the enzyme activities were expressed as μmol g^{-1} soil h^{-1}. Six blanks and controls were included to correct for background absorbance.

The activities of BG, CBH, and AP were measured using p-nitrophenyl (pNP) substrates (Alef and Nannipieri 1995; German et al. 2011; Tabatabai and Bremner 1969). Fresh soil (1 g) was incubated at 37 °C for 1 h with 4 mL buffer and 1 mL substrate solution. Specifically, the BG assays used a modified universal buffer (pH 6.0) with 0.05 M of p-nitrophenyl-β-D-glucopyranoside (pNPG); the CBH assays used a 50 mM acetate buffer (pH 5.5) with 0.025 M p-nitrophenyl-β-D-cellobioside (pNPC); and the AP assays employed a modified universal buffer (pH 6.5) with 0.05 M p-nitrophenyl phosphate (pNPP). The reactions were terminated by adding 1 mL of 0.5 M $CaCl_2$ and 4 mL of an alkaline solution (0.1 M Tris, pH 12.0 for BG; 0.1 M NaOH for CBH; 0.5 M NaOH for AP), followed by centrifugation. The release of p-nitrophenol (PNP) was quantified spectrophotometrically (400 nm for BG and CBH; 410 nm for AP).

The PO activity was assayed following the method described by German et al. (2011) using L-DOPA as the reaction substrate. Briefly, 1 g of fresh soil was suspended in 5 mL of 50 mM sodium acetate buffer (pH 5.0), after which 1 mL of 25 mM L-DOPA solution was added to initiate the reaction. The mixture was incubated at 25 °C in darkness for 20 min and subsequently centrifuged to obtain the supernatant. The formation of dopachrome was then measured spectrophotometrically at 460 nm.

2.9 Quantification of *GH48* and *cbh*I abundance and community composition

The soil DNA was extracted from 0.5 g of fresh soil using the FastDNA™ Spin Kit for Soil (MP Biomedicals, USA) according to the manufacturer's instructions. The DNA concentration and purity were measured with a NanoDrop 2000 spectrophotometer (Thermo Fisher Scientific, USA). Quantitative PCR (qPCR) was performed to determine the absolute abundances of *GH48* and *cbh*I genes. Each 20 μL reaction contained 10 μL of SYBR Green Master Mix (Applied Biosystems, USA), 0.5 μM of forward and reverse primers specific for *GH48* or *cbh*I, 2 μL of template DNA, and nuclease-free water. Thermal cycling conditions included initial denaturation at 95 °C for 3 min; 35 cycles of 95 °C for 30 s, 55 °C for 30 s, and 72 °C for 45 s; followed by a melting curve analysis. Standard curves were generated using serial dilutions of plasmids that contained cloned target gene fragments, while gene copy numbers were expressed as copies per gram of dry soil.

To determine the composition of the functional gene community, PCR amplicons of *GH48* and *cbh*I were

generated from the soil DNA using primers with sample-specific barcodes. The amplicons were purified and sequenced using an Illumina MiSeq platform (Shanghai Majorbio Bio-Pharm Technology Co., Ltd, China) with the TruSeq™ DNA Sample Preparation Kit. Raw sequences were processed using QIIME 2, and amplicon sequence variants (ASVs) were generated using the DADA2 denoising algorithm. Taxonomic assignments were performed against a curated *GH48* and *cbh*I reference database, and the relative abundances of detected phyla were calculated to reveal the functional gene community structure at the phylum level.

2.10 Statistical analyses

Statistical analyses were performed using R 4.5.1 (R Core Team 2025) and Origin 2025 (OriginLab, USA). Data normality and variance homogeneity were checked via the Shapiro–Wilk and Levene's tests, respectively. One-way ANOVA with Tukey's HSD was used to evaluate the effects of fertilization on cumulative soil-derived CO_2 under each temperature, while two-way ANOVA assessed the influences of fertilization and the C pool on Q_{10}.

Pearson correlation analysis was conducted to examine the relationships between the soil-derived CO_2 and soil variables, including substrate availability (WEOC, available P, and the WEOC/available P ratio), substrate quality (alkyl C, O-alkyl C, aromatic C, and carbonyl C), enzyme activities (BG, CBH, PO, and AP), and microbial properties (MBC, *GH48*, and *cbh*I gene abundance). To investigate how inherent soil characteristics influenced Q_{10} under warming, correlations between soil variables measured at 25 °C and Q_{10} were assessed. Variables that showed significant correlations with Q_{10} ($P<0.05$) were included in a Random Forest (RF) model to assess their relative contributions to Q_{10} variability. The RF analysis was performed using the randomForest package in R with 500 trees and mtry set to one-third of the predictors. Variable importance was evaluated based on the percent increase in mean square error (%IncMSE). Given the limited sample size ($n=18$), the results should be interpreted cautiously due to potential model instability and overfitting.

The responses of each soil variable to fertilization, relative to the control, were quantified using the natural log response ratio (ln *RR*), calculated as:

$$\ln RR = \ln\left(\frac{X_F}{X_C}\right) \tag{6}$$

where X_F and X_C are the means of the fertilized and control treatments, respectively. The standard error (SE) of ln *RR* was estimated following Hedges et al. (1999):

$$SE_{\ln RR} = \sqrt{\frac{SD_F^2}{n_F X_F^2} + \frac{SD_C^2}{n_C X_C^2}} \tag{7}$$

where SD_F and SD_C are the standard deviations, while n_F and n_C are the sample sizes for the fertilized and control treatments, respectively. For each ln*RR* estimate, a 95% confidence interval (CI) was calculated as:

$$95\%CI = \ln RR \pm t_{\alpha/2,df} \times SE_{\ln RR} \tag{8}$$

with $t_{\alpha/2,\ df}$ being the critical value from the *t*-distribution at $df=n_F+n_C-2$. A given response was considered statistically significant when the 95% CI did not include zero.

The above method was chosen because the absolute values of soil variables at 25 °C were already reported in Jiang et al. (2026a) based on the same experimental system. To avoid duplication of previously published baseline data, we used ln *RR* to focus on the relative changes induced by fertilization, enabling direct comparison of treatment effects across temperatures.

3 Results

3.1 Soil-derived CO_2 and Q_{10}

At the end of incubation (day 56), CP increased the cumulative soil-derived CO_2 by 31–36% relative to the control, whereas NanoBP reduced it by 11–18% (Fig. 1a). Warming stimulated the soil-derived CO_2 release for all treatments, with increases of 68% for the control, 75% for CP, and 55% for NanoBP (Fig. 1a).

Both the single- and double-exponential decay models provided excellent fits to the data, with adj $R^2>0.98$ and $P<0.001$ (Table S1), indicating that both models could reliably capture the dynamics of SOC mineralization. Soil-derived CO_2 emissions demonstrated consistent patterns across the bulk soil, active C pool, and slow C pool (Fig. 1b–d). Specifically, CP increased CO_2 emissions from the bulk soil, active C, and slow C pools by 31–35%, 31–36%, and 31–34% compared with the control, respectively (Fig. 1b–d). In contrast, NanoBP reduced the emissions from these pools by 11–18%. Warming enhanced CO_2 release from the bulk soil by 54–73%, active C pool by 55–74%, and slow C pool by 54–72% (Fig. 1b–d).

The effects on Q_{10} differed between the treatments. The CP had no significant influence on Q_{10} in any of the three C pools, whereas NanoBP consistently reduced Q_{10} by 8% for the bulk soil, active C pool, and slow C pool, respectively (Fig. 2). No significant differences in Q_{10} were observed between the three C pools under the same treatment (Fig. 2).

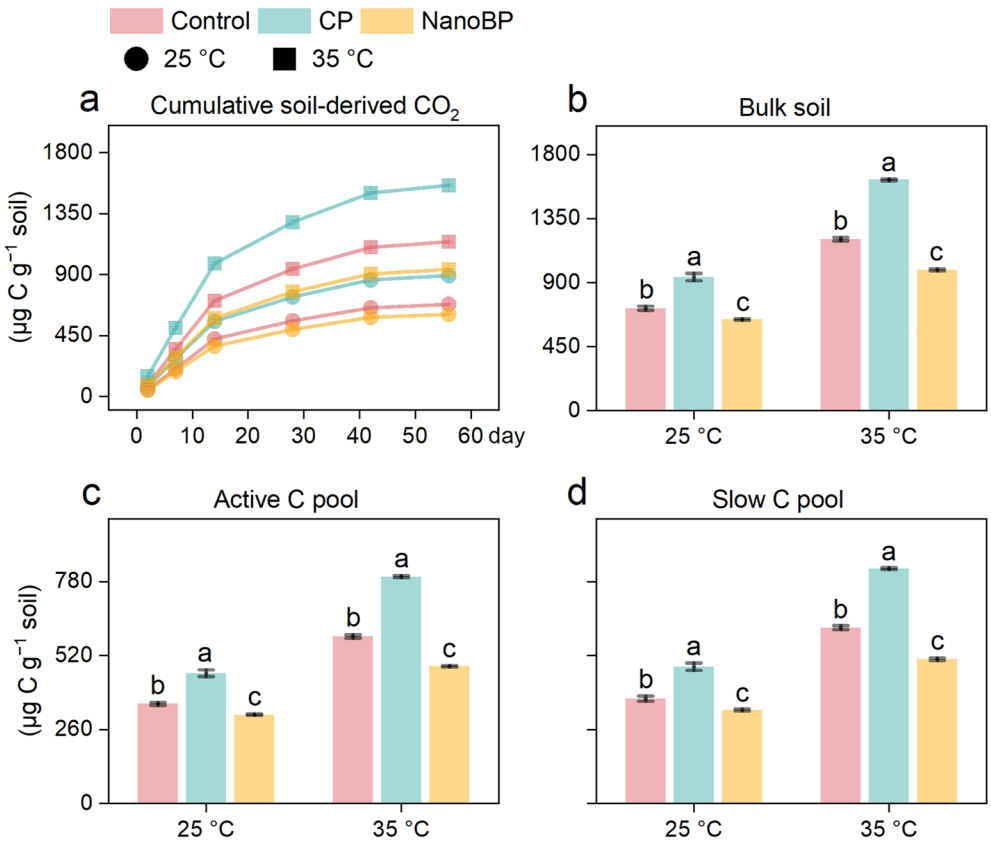

Fig. 1 **a** Cumulative soil-derived CO_2 emissions; soil-derived CO_2 emissions from **b** bulk soil estimated using a first-order kinetic one-compartment model, from **c** the active carbon (C) pool, and **d** the slow C pool estimated using a two-pool model. Different lowercase letters indicate significant differences between the three P treatments at 25 °C or 35 °C. Error bars are ± standard errors ($n = 3$). Control, no fertilizer; CP, chemical phosphorus fertilizer; NanoBP, nanozeolite-coupled biochar-based phosphate fertilizer

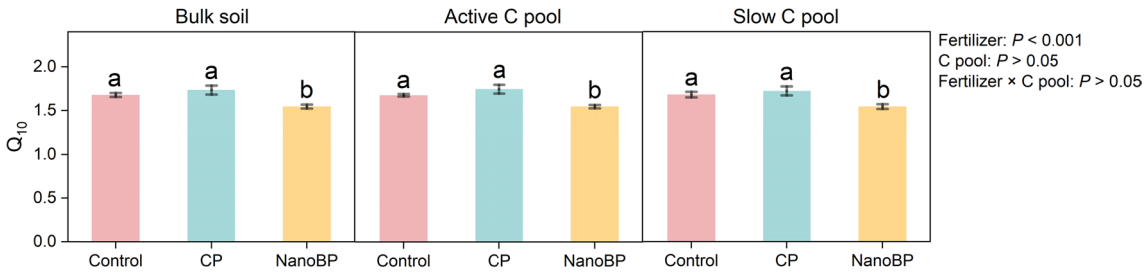

Fig. 2 Temperature sensitivity of soil organic carbon (C) mineralization (Q_{10}) for bulk soil, active C pool, and slow C pool. Different lowercase letters indicate significant differences between the fertilization treatments. Values are means ± standard errors ($n = 3$). Control, no fertilizer; CP, chemical phosphorus fertilizer; NanoBP, nanozeolite-coupled biochar-based phosphate fertilizer

3.2 Soil variables

Relative to the control, CP decreased the soil pH by 0.15–0.16 units, while NanoBP increased the pH by 0.29–0.31 units (Fig. 3a and b). Both CP and NanoBP increased WEOC relative to the control; however, the enhancement was substantially greater under NanoBP (61–62%) than under CP (11–12%). Similarly, available P rose by 146–147% under CP and by 171–172% under NanoBP (Fig. 3a, b). Despite these increases, the WEOC/available P ratio declined under both P-added treatments, with a larger reduction under CP (55%) than NanoBP (40–41%; Fig. 3a and b).

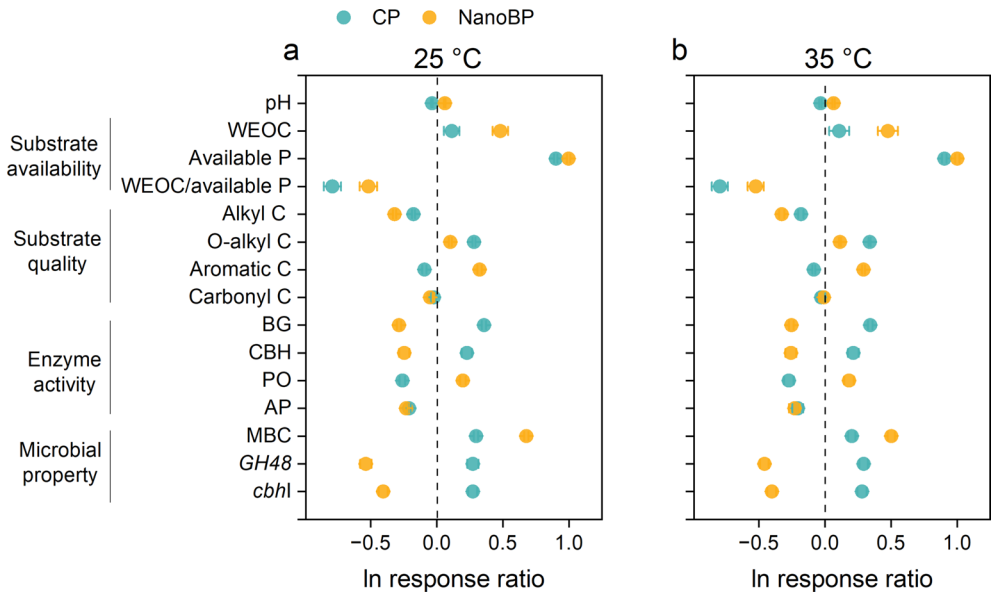

Fig. 3 Response ratios of soil variables to chemical phosphorus fertilizer (CP) and nanozeolite-coupled biochar-based phosphate fertilizer (NanoBP) under **a** 25 °C and **b** 35 °C. Substrate availability includes water-extractable organic carbon (WEOC), available phosphorus (P), and the WEOC/available P ratio; substrate quality includes alkyl carbon (C), O-alkyl C, aromatic C, and carbonyl C; enzyme activity includes β-glucosidase (BG), cellobiohydrolase (CBH), polyphenol oxidase (PO), and acid phosphatase (AP); microbial properties include microbial biomass C (MBC), *GH48*, and *cbh*I abundance. Values are log-transformed response ratios with 95% confidence intervals (CI); responses are considered significant when the 95% CI does not overlap with zero ($P < 0.05$)

Relative to the control, fertilization also shifted the chemical composition of SOC (Fig. 3a and b). Alkyl C decreased under both the CP (16–17%) and NanoBP (27–28%; Fig. 3a and b). O-alkyl C increased in both cases, albeit with a stronger effect under CP (33–40%) than NanoBP (11–12%; Fig. 3a and b). The two fertilizers had opposing effects on aromatic C; CP reduced it by 8–9%, while NanoBP increased it by 34–38%. Neither treatment altered the carbonyl C (Fig. 3a and b).

The enzyme activities responded divergently to CP and NanoBP (Fig. 3a and b), with CP increasing the activities of BG and CBH by 41–43% and 24–26% compared with the control, respectively, while NanoBP decreased them by 22–25% and 22–23%, respectively (Fig. 3a and b). While opposite effects on PO activities were observed, the AP activities declined under both CP (19%) and NanoBP (20%), with no difference between the two P types (Fig. 3a and b).

Soil MBC and abundances of C-degrading genes also shifted (Fig. 3a and b). The MBC increased by 23–35% under CP and 65–97% under NanoBP (Fig. 3a and b). In contrast, CP increased *GH48* by 31–34%, whereas NanoBP decreased it by 37–42%. The *cbh*I abundance followed the same pattern as *GH48* as a function of P treatment type (Fig. 3a and b).

Importantly, all fertilization responses described above were consistent at both 25 °C and 35 °C (Fig. 3a and b).

3.3 Factors influencing soil-derived CO_2 and Q_{10}

Across all three C pools (bulk soil, active and slow C pools), neither the pH nor substrate availability metrics (WEOC, available P, and WEOC/available P ratio) were correlated with soil-derived CO_2 ($P > 0.05$; Fig. 4a). Among substrate quality indicators, only carbonyl C exhibited a negative correlation with soil-derived CO_2 ($r = -0.68$ to -0.69, $P < 0.01$; Fig. 4a). Conversely, the activities of BG ($r = 0.70$, $P < 0.01$) and CBH ($r = 0.62$–0.63, $P < 0.01$) were positively correlated with soil-derived CO_2 release, while PO and AP activities showed no relationship ($P > 0.05$; Fig. 4a). In terms of microbial functional genes, the abundances of *GH48* ($r = 0.79$–0.80, $P < 0.01$) and *cbh*I ($r = 0.50$–0.51, $P < 0.01$) were positively associated with soil-derived CO_2 emissions, while MBC showed no significant correlation (Fig. 4a).

The Q_{10} was negatively correlated with soil pH across all C pools ($r = -0.30$ to -0.76, $P < 0.05$), but not with the substrate availability parameters ($P > 0.05$; Fig. 4b). Within the substrate quality metrics, only aromatic C negatively correlated with Q_{10} ($r = -0.77$ to -0.80, $P < 0.05$; Fig. 4b). The Q_{10} was positively associated with the activities of BG ($r = 0.74$–0.79, $P < 0.05$) and CBH ($r = 0.73$–0.78, $P < 0.05$) but negatively with the PO activity ($r = -0.81$ to -0.85, $P < 0.01$; Fig. 4b). The abundances of *GH48* ($r = 0.77$–0.80, $P < 0.01$) and *cbh*I ($r = 0.82$–0.86,

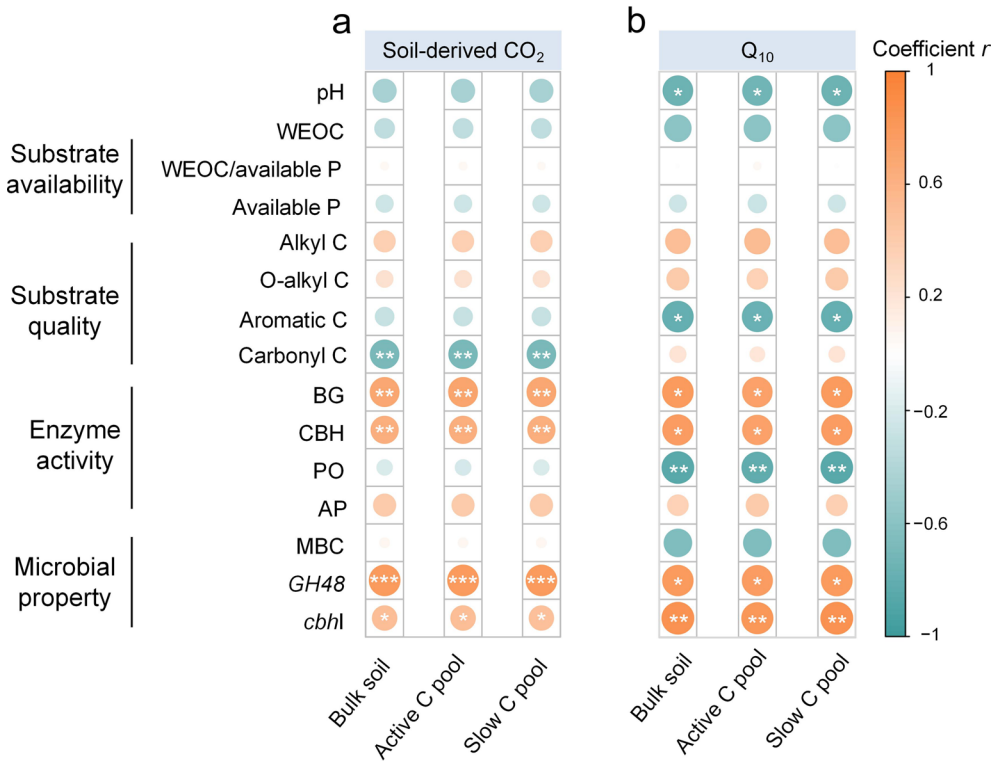

Fig. 4 Relationships between **a** soil-derived CO_2 and soil variables from bulk soil, the active carbon (C) pool, and the slow C pool ($n = 18$), and **b** temperature sensitivity of soil organic C mineralization (Q_{10}) and soil variables at 25 °C ($n = 9$). Substrate availability includes water-extractable organic carbon (WEOC), available phosphorus (P), and the WEOC/available P ratio; substrate quality includes alkyl C, O-alkyl C, aromatic C, and carbonyl C; enzyme activity includes β-glucosidase (BG), cellobiohydrolase (CBH), polyphenol oxidase (PO), and acid phosphatase (AP); microbial properties include microbial biomass C (MBC), *GH48*, and *cbh*I abundance. *, $P < 0.05$; **, $P < 0.01$; ***, $P < 0.001$

$P < 0.01$) were also positively related to Q_{10}, while MBC showed no significant relationship (Fig. 4b).

3.4 Key factors regulating Q_{10}

Random forest analysis identified the abundance of *cbh*I, as well as BG and CBH activities as the most influential variables of Q_{10} variability in bulk soil (Fig. 5a). For the active C pool, *cbh*I and *GH48* abundances, together with BG activity, were the most important variables (Fig. 5b). For the slow C pool, BG activity, *cbh*I abundance, and PO activity emerged as the top variables (Fig. 5c).

Given the strong associations between functional gene abundance and Q_{10}, we examined the taxonomic composition of *GH48*- and *cbh*I-associated communities. However, community composition varied only slightly among the treatments, and its relationship with Q_{10} was weak compared with the effects on gene abundances (Fig. 5d–f). Therefore, Q_{10} variation in this study appears to be more closely linked to functional gene abundance than to major shifts in taxonomic structure.

4 Discussion

This study examined how NanoBP and CP influenced SOC mineralization and its Q_{10} in an intensively managed Moso bamboo forests. Although both P treatments supplied comparable amounts of P, NanoBP led to lower SOC mineralization rates and Q_{10} values across C pools compared with the control, whereas CP increased SOC-derived CO_2 emissions without altering Q_{10}. These contrasting patterns suggest that P form, rather than P input alone, influences how fertilization regulates microbial C processing and Q_{10}.

4.1 Phosphorus form rather than phosphorus input is associated with contrasting Q_{10} responses under NanoBP and CP

Despite comparable P inputs, NanoBP and CP produced contrasting effects on SOC mineralization and Q_{10} (Figs. 1 and 2), indicating that total P supply alone did not fully explain decomposition responses. Chemical P fertilizer provides readily soluble orthophosphate that can rapidly alleviate microbial P limitation in highly weathered subtropical soils (Shi et al. 2023). In this study, CP increased SOC-derived CO_2 emissions and

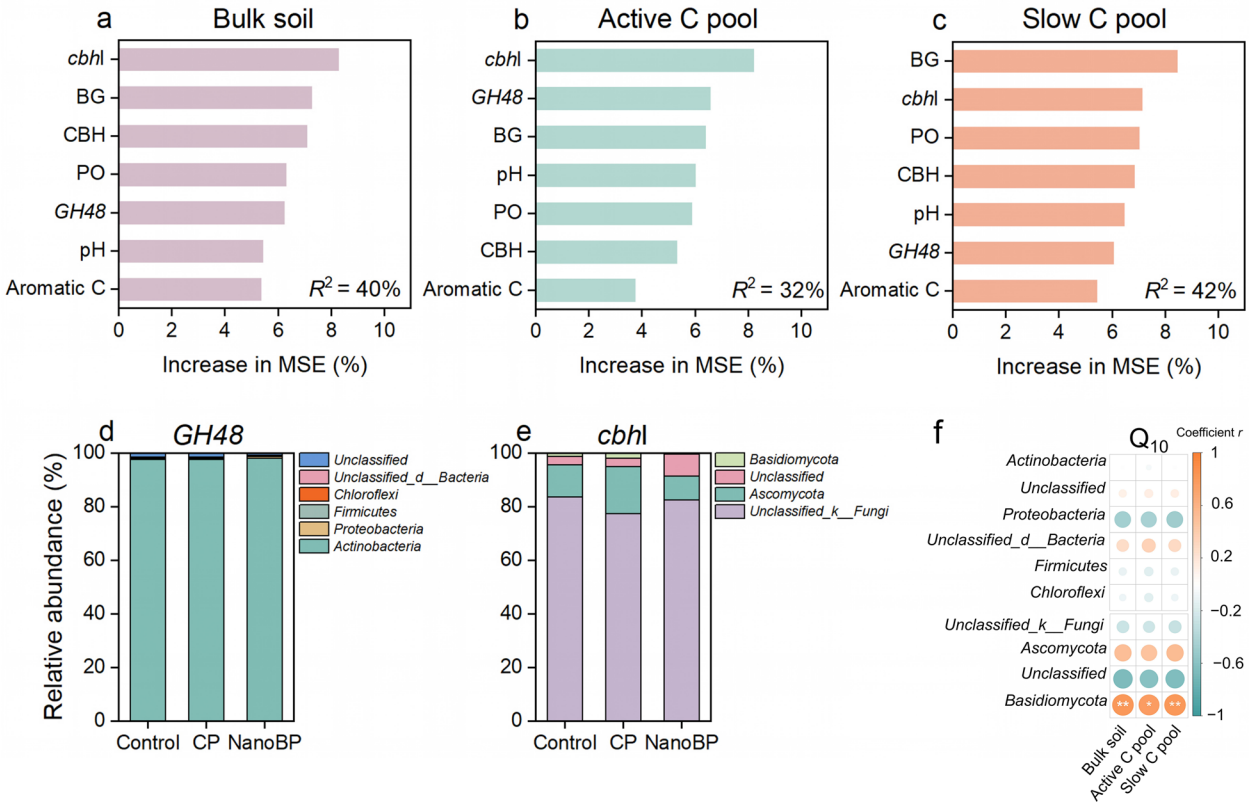

Fig. 5 Importance of predictors for the temperature sensitivity of soil organic carbon (C) mineralization (Q_{10}), based on Random Forest models for **a** bulk soil, **b** the active C pool, and **c** the slow C pool; the relative abundances of **d** *GH48* and **e** *cbhI*; and relationships between Q_{10} and the relative abundances of *GH48* and *cbhI*. MSE, mean squared error; BG, β-glucosidase; CBH, cellobiohydrolase; PO, polyphenol oxidase. Control, no fertilizer; CP, chemical phosphorus fertilizer; NanoBP, nanozeolite-coupled biochar-based phosphate fertilizer. *, $P < 0.05$; **, $P < 0.01$

available P relative to the control (Figs. 1 and 3), consistent with the stimulation of immediate P availability in SOC decomposition (Han et al. 2026). However, this stimulation occurred proportionally at both incubation temperatures, resulting in little change in Q_{10} (Fig. 2). These findings suggest that immediate P supply enhanced microbial activity (e.g., MBC) but may not have substantially altered the physicochemical constraints governing Q_{10}.

In contrast, P in NanoBP is embedded within a composite matrix composed of nanozeolite, biochar, and mineral components (Dong et al. 2025). The nanozeolite fraction provides a high specific surface area and reactive aluminosilicate domains, whereas biochar contributes porous C structures, alkalinity, functional groups, and organo–mineral interfaces (Jiang et al. 2026b; Li et al. 2025; Wu et al. 2025; Zhou et al. 2026b). Together, these components may create heterogeneous sorption sites and diffusion pathways that influence P retention and the spatial accessibility of organic substrates (Shahjahan et al. 2025; Yuan et al. 2025).

Consistent with this interpretation, NanoBP increased available P (Fig. 3) but resulted in lower SOC mineralization rates than CP (Fig. 1), indicating that enhanced P availability alone did not stimulate CO_2 emission (Nottingham et al. 2015). One possible explanation is that the composite structure of NanoBP alters the physicochemical context in which SOC decomposition occurs. Mineral components such as kaolinite, together with the porous surfaces of biochar and nanozeolite, may provide additional sorption sites that promote organo–mineral associations (Miranda-Trevino and Coles 2003). These interactions can reduce the accessibility of organic substrates to decomposers, thereby constraining SOC mineralization. Reduced substrate accessibility may also dampen the response of decomposition to warming (Conant et al. 2011).

Moreover, NanoBP further elevated soil pH, a response attributable to the inherently alkaline nature of its biochar fraction (Fig. 3). Changes in soil pH can influence mineral surface charge, P sorption equilibria, and organo–mineral interactions in acid soils, thereby potentially affecting substrate accessibility and decomposition

processes (Malik et al. 2018). The negative correlation between soil pH and Q_{10} across treatments (Fig. 4) suggests that the NanoBP-induced amelioration of soil acidity may have contributed to the reduced Q_{10} observed under NanoBP.

Taken together, these structural and chemical characteristics indicate that NanoBP likely functions not only as a P source but also as a material that modifies the physicochemical environment of decomposition and moderates its response to warming compared with soluble P fertilizer.

4.2 Variations in Q_{10} are more closely linked to microbial functional traits than to substrate availability

While differences in materials and soil physicochemical properties may explain treatment-level contrasts in Q_{10}, the variation in Q_{10} across the treatments was more closely associated with microbial functional traits than with substrate availability per se. Across the treatments, Q_{10} showed weak relationships with the substrates, including WEOC and available P (Fig. 4), consistent with previous studies suggesting that substrate pool size alone is often a poor predictor of Q_{10} (Conant et al. 2011).

The composite structure of NanoBP may have indirectly influenced microbial functional expression by modifying microsite nutrient dynamics and substrate accessibility (Dong et al. 2025). Spatial constraints of P release and mineral-associated SOC could alter microbial resource conditions without proportionally increasing C mineralization (Enebe et al. 2025). Although available P did not show significant relationships with Q_{10} across the treatments, P availability can still influence microbial metabolic strategies and enzyme allocation patterns (Chen et al. 2024). Previous studies have shown that alleviation of P limitation may reduce microbial investment in C-acquiring enzymes, thereby moderating SOC mineralization responses to warming (Bednik et al. 2023; Fanin et al. 2022). In this context, the elevated available P observed under NanoBP may have contributed to shifts in microbial metabolic allocation rather than directly controlling Q_{10}. Under such conditions, microbial communities may adjust resource allocation strategies and reduce investment in extracellular enzyme production for C acquisition (German et al. 2012; Whalen et al. 2024).

Consistent with this interpretation, the NanoBP treatment exhibited reduced activities of BG and CBH and reduced abundances of cellulolytic functional genes such as *GH48* and *cbh*I (Fig. 4), which emerged as important predictors in the Random forest analysis (Fig. 5). Because extracellular depolymerization is widely regarded as a rate-limiting step in SOC decomposition, the decreased investment in enzyme production may have moderated SOC mineralization and attenuated its responsiveness to increasing temperature (Alvarez et al. 2018; Fanin et al. 2022). These findings are broadly consistent with trait-based microbial frameworks in which Q_{10} emerges from shifts in enzyme production and resource allocation rather than from changes in substrate quantity alone (Allison et al. 2010; Frey et al. 2013). Thus, the proximate regulation of Q_{10} in this study appears to reflect variation in microbial functional expression.

4.3 Reduced Q_{10} of slow C pools under NanoBP may reflect accessibility constraints

Theoretical frameworks often predict higher Q_{10} values for chemically complex SOC due to greater energy requirements (Bosatta and Ågren 1999; Craine et al. 2010). However, in this study, Q_{10} values did not differ markedly between active and slow C pools across the treatments (Fig. 2), suggesting that chemical recalcitrance alone did not dominate Q_{10} patterns in this bamboo forest soil. Instead, both pools appeared subject to similar accessibility and enzymatic constraints. This outcome may also reflect limitations of model structure and incubation duration, and should not be interpreted as definitive evidence of thermodynamic equivalence among distinct SOC fractions.

Notably, NanoBP lowered Q_{10} for the slow C pool despite higher proportions of aromatic C (Fig. 2). This apparent mismatch suggests that factors beyond intrinsic chemical recalcitrance may influence Q_{10}. One possible explanation is that the biochar–nanozeolite matrix altered the physicochemical accessibility of organic substrates, potentially enhancing sorption interactions or microstructural protection (Jiang et al. 2026a; Raut et al. 2025). If diffusion constraints or substrate accessibility limitations became more prominent, decomposition rates may have been less responsive to temperature increases, leading to lower apparent Q_{10} values (Li et al. 2013; Moinet et al. 2018). However, as sorption capacity, pore structure, and enzyme diffusion were not directly measured in this study, this interpretation should be considered plausible and requires further experimental verification.

The concurrent reduction in cellulolytic enzyme activities and functional gene abundances (Fig. 3) further supports the proposition that microbial exploitation of slow SOC pools was constrained under NanoBP. These combined physicochemical and biological constraints may outweigh the intrinsic thermodynamic sensitivity of chemically complex SOC.

4.4 Implications for nano-enabled phosphate fertilizer design in bamboo systems

This study showed that NanoBP may influence SOC dynamics not only by supplying nutrients but also by modifying Q_{10}. In intensively managed bamboo forests, CP application increased SOC mineralization without substantially altering Q_{10}, which may contribute to enhanced C losses under future warming scenarios (Sun et al. 2018). In contrast, NanoBP lowered SOC mineralization rates and Q_{10}, indicating a potential to moderate warming-induced C losses while maintaining P availability.

From a fertilizer design perspective, NanoBP may offer a pathway to decouple P supply from accelerated soil C loss. By embedding P within nanozeolite-coupled biochar–mineral matrices, fertilizer functionality can extend beyond nutrient delivery to include regulation of microbial access to C substrates (Wu et al. 2025). This implies that future fertilizer development could integrate material properties, such as surface reactivity and pore structure, as design variables (e.g., modifying specific surface area or tailoring pore size distribution to regulate nutrient diffusion and microbial access) to influence belowground biogeochemical processes, rather than focusing solely on nutrient release kinetics.

At the evaluation level, Q_{10} emerges as a potentially informative indicator for assessing the climate-relevant impacts of novel fertilizers. Fertilizers that maintain crop nutrient supply while reducing Q_{10} may help limit unintended increases in soil C loss under warming. Incorporating Q_{10} alongside conventional agronomic metrics could therefore support more comprehensive screening of NanoBP formulations, particularly in high-input systems characterized by rapid C turnover. For industrial bamboo systems and other intensively managed perennial crops, these implications are especially relevant. Such systems require sustained nutrient inputs to support their high productivity, yet they also exhibit strong microbial activity and sensitivity of soil C cycling to management (Zhou et al. 2024, 2026a). NanoBP designed to moderate Q_{10} may contribute to reconciling productivity demands with soil C conservation goals. While field validation is required, this study provides a process-based rationale for considering NanoBP design as part of climate-resilient nutrient management strategies in industrial crop production.

It should be noted that this study did not directly track nanoparticle dispersion or quantify nanoscale interactions in soil. The nanozeolite was incorporated into granulated composite particles during fertilizer formulation, and its role was inferred from retained surface and structural properties within the composite, rather than from free nanoparticle mobility. The study evaluated formulation-level effects of a multi-component material (biochar, nano-zeolite, kaolinite, and phosphate) without single-component controls to resolve individual effects. The observed short-term effects on CO_2 release and Q_{10} under controlled conditions represent changes in temperature responsiveness, rather than long-term SOC stabilization, which is confounded by plant growth, root–microbe interactions, aggregation dynamics, and environmental heterogeneity. Additionally, kinetic models partition SOC into operational pools based on fitted parameters, and the absence of clear Q_{10} differences may reflect model structure, parameter uncertainty, or incubation duration.

The use of a constant 35 °C treatment could impose physiological stress on microbial taxa, potentially influencing apparent Q_{10}. Furthermore, using just two temperatures (25 °C and 35 °C) to calculate a single Q_{10} assumes constant temperature sensitivity across this 10 °C range, which may not hold true, particularly when treatments alter the temperature response curve. Finally, only a single P application rate was tested, so formulation effects cannot be separated from possible dose responses. These limitations suggest that the findings should be interpreted as evidence of composite-fertilizer influences under controlled conditions. Future studies with broader temperature ranges, multiple treatments, factorial controls, varying application rates, and advanced imaging or isotope tracing are needed to clarify in situ mechanisms and field-scale relevance.

5 Conclusion

This study revealed that P fertilization regulated Q_{10} in bamboo forest soils, with chemical fertilizer accelerating SOC mineralization without altering Q_{10}, while NanoBP lowered both SOC mineralization and Q_{10} of slow C pool during short-term incubation. The Q_{10} was controlled primarily by cellulolytic enzyme activities and functional gene abundances, rather than by substrate supply, with BG, CBH, *GH48*, and *cbh*I as key determinants. Our findings indicate that formulation of NanoBP may provide a pathway to moderate soil C losses under warming. Future research should assess the persistence of these effects under field conditions and diverse management regimes.

Supplementary Information

The online version contains supplementary material available at https://doi.org/10.1007/s42773-026-00620-0.

Additional file 1.

Author contributions
Zhenhui Jiang: Investigation, Methodology, Writing—original draft, Writing—review & editing. Caixian Tang: Writing—review & editing. Yunying Fang: Writing—review & editing. Tida Ge: Writing—review & editing. Shuokang Liu: Investigation, Methodology. Yu Luo: Writing—review & editing. Bing Yu: Writing—review & editing. Yanjiang Cai: Writing—review & editing. Jason C. White: Writing—review & editing. Yongfu Li: Supervision, Writing— original draft, Writing—review & editing. All authors read and approved the final manuscript.

Funding
This study was supported by the National Key Research and Development Program of China (No. 2022YFE0127800), and National Natural Science Foundation of China (No. 32271845, U24A20429).

Data availability
Data will be made available on reasonable request.

Declarations

Competing interests
Yu Luo is an EBM of the journal Biochar, and he was not involved in the peer-review or handling of the manuscript. The authors declare that they have no known competing financial interests or personal relationships that might have appeared to influence the work reported in this paper.

Author details
[1]State Key Laboratory for Development and Utilization of Forest Food Resources, College of Environmental and Resource Sciences, Zhejiang A&F University, Hangzhou 311300, China. [2]Department of Ecological, Plant and Animal Sciences, La Trobe Institute for Sustainable Agriculture and Food, La Trobe University, Bundoora, VIC 3086, Australia. [3]Australian Rivers Institute and School of Environment and Science, Griffith University, Nathan, QLD 4111, Australia. [4]State Key Laboratory for Quality and Safety of Agro-Products, International Science and Technology Cooperation Base for the Regulation of Soil Biological Functions and One Health of Zhejiang Province, Ningbo University, Ningbo 315211, China. [5]College of Environmental and Resource Science, Zhejiang University, Hangzhou 310058, China. [6]The Connecticut Agricultural Experiment Station, 123 Huntington Street, New Haven, CT 06511, USA.

Received: 7 January 2026 Revised: 27 March 2026 Accepted: 13 April 2026
Published online: 15 June 2026

References

Alef K, Nannipieri P (1995) Methods in applied soil microbiology and biochemistry. Academic Press, London
Allison SD, Wallenstein MD, Bradford MA (2010) Soil-carbon response to warming dependent on microbial physiology. Nat Geosci 3:336–340. https://doi.org/10.1038/ngeo846
Alvarez G, Shahzad T, Andanson L, Bahn M, Wallenstein MD, Fontaine S (2018) Catalytic power of enzymes decreases with temperature: new insights for understanding soil C cycling and microbial ecology under warming. Glob Chang Biol 24:4238–4250. https://doi.org/10.1111/gcb.14281
Bednik M, Medyńska-Juraszek A, Ćwieląg-Piasecka I, Dudek M (2023) Enzyme activity and dissolved organic carbon content in soils amended with different types of biochar and exogenous organic matter. Sustainability 15:15396. https://doi.org/10.3390/su152115396
Bosatta E, Ågren GI (1999) Soil organic matter quality interpreted thermodynamically. Soil Biol Biochem 31:1889–1891. https://doi.org/10.1016/S0038-0717(99)00105-4
Bray RH, Kurtz LT (1945) Determination of total, organic, and available forms of phosphorus in soils. Soil Sci 59:39–46
Chen K, Zhou H, Wu Y, Zhao Z, Li Y, Qiao L, Liu G, Xue S (2022) Effects of long-term nitrogen and phosphorus fertilization on soil microbial, bacterial and fungal respiration and their temperature sensitivity on the Qinghai-Tibet Plateau. PeerJ 10:e12851. https://doi.org/10.7717/peerj.12851
Chen C, Pei J, Li B, Fang C, Nie M, Li J (2024) Nutrient addition enhances the temperature sensitivity of soil carbon decomposition across forest ecosystems. Glob Chang Biol 30:e17543. https://doi.org/10.1111/gcb.17543
Conant RT, Ryan MG, Ågren GI, Birge HE, Davidson EA, Eliasson PE, Evans SE, Frey SD, Giardina CP, Hopkins FM, Hyvönen R, Kirschbaum MUF, Lavallee JM, Leifeld J, Parton WJ, Steinweg JM, Wallenstein MD, Wetterstedt JAM, Bradford MA (2011) Temperature and soil organic matter decomposition rates: synthesis of current knowledge and a way forward. Glob Chang Biol 17:3392–3404. https://doi.org/10.1111/j.1365-2486.2011.02496.x
Craine JM, Spurr R, McLauchlan K, Fierer N (2010) Landscape-level variation in temperature sensitivity of soil organic carbon decomposition. Soil Biol Biochem 42:373–375. https://doi.org/10.1016/j.soilbio.2009.10.024
Crowther TW, Todd-Brown KEO, Rowe CW, Wieder WR, Carey JC, Machmuller MB, Snoek BL, Fang S, Zhou G, Allison SD, Blair JM, Bridgham SD, Burton AJ, Carrillo Y, Reich PB, Clark JS, Classen AT, Dijkstra FA, Elberling B, Emmett BA, Estiarte M, Frey SD, Guo J, Harte J, Jiang L, Johnson BR, Kroel-Dulay G, Larsen KS, Laudon H, Lavallee JM, Luo Y, Lupascu M, Ma LN, Marhan S, Michelsen A, Mohan J, Niu S, Pendall E, Penuelas J, Pfeifer-Meister L, Poll C, Reinsch S, Reynolds LL, Schmidt IK, Sistla S, Sokol NW, Templer PH, Treseder KK, Welker JM, Bradford MA (2016) Quantifying global soil carbon losses in response to warming. Nature 540:104–108. https://doi.org/10.1038/nature20150
Dong C, Cheng Y, Wu M, Wang Q, Zhang Y, White JC, Xiang H, Cai Y, Li Y, Yu B (2025) Nanozeolite-coupled biochar-based controlled-release phosphorus fertilizer: performance, release mechanism, and techno-economic analysis. ACS Sustain Chem Eng 13:3785–3796. https://doi.org/10.1021/acssuschemeng.4c10901
Duan P, Wang C, Wanek W, Yang X, Hu P, Wang K, Li D (2025) Soil microbial phosphorus limitation constrains carbon use efficiency in subtropical forests. Soil Biol Biochem 210:109937. https://doi.org/10.1016/j.soilbio.2025.109937
Enebe MC, Ray RL, Griffin RW (2025) The impacts of biochar on carbon sequestration, soil processes, and microbial communities: a review. Biochar 7:10. https://doi.org/10.1007/s42773-025-00432-8
Fanin N, Mooshammer M, Sauvadet M, Meng C, Alvarez G, Bernard L, Bertrand I, Blagodatskaya E, Bon L, Fontaine S, Niu S, Lashermes G, Maxwell TL, Weintraub MN, Wingate L, Moorhead D, Nottingham AT (2022) Soil enzymes in response to climate warming: mechanisms and feedbacks. Funct Ecol 36:1378–1395. https://doi.org/10.1111/1365-2435.14027
Feng S, Zhang P, Hu Y, Jin F, Liu Y, Cai S, Song Z, Zhang X, Nadezhda T, Guo Z, Lynch I, Dang X (2022) Combined application of biochar and nanozeolite enhanced cadmium immobilization and promote the growth of Pak Choi in cadmium contaminated soil. NanoImpact 28:100421. https://doi.org/10.1016/j.impact.2022.100421
Frey SD, Lee J, Melillo JM, Six J (2013) The temperature response of soil microbial efficiency and its feedback to climate. Nat Clim Change 3:395–398. https://doi.org/10.1038/nclimate1796
German DP, Weintraub MN, Grandy AS, Lauber C, Rinkes ZL, Allison SD (2011) Optimization of hydrolytic and oxidative enzyme methods for ecosystem studies. Soil Biol Biochem 43:1387–1397. https://doi.org/10.1016/j.soilbio.2011.03.017
German DP, Marcelo KRB, Stone MM, Allison SD (2012) The Michaelis-Menten kinetics of soil extracellular enzymes in response to temperature: a cross-latitudinal study. Glob Chang Biol 18:1468–1479. https://doi.org/10.1111/j.1365-2486.2011.02615.x
Gul J, Khan MNA, Sikander U, Khoja AH, Kah M, Naqvi SR (2026) Machine learning optimization for algal biochar yield: integrating experimental validation and sensitivity analysis. Biochar 8:8. https://doi.org/10.1007/s42773-025-00511-w
Han G, Asghar RMA, Khan AA, Chen Y, Wang J, Wei S, Liu C, Li Z, Wang Z, Huang D, Wei X, Cao W, Gao Y, Zhang D (2026) Enhance soil phosphorus availability via the growth and decomposition of green manure crops in drylands. Soil Tillage Res 257:106919. https://doi.org/10.1016/j.still.2025.106919
Hedges LV, Gurevitch J, Curtis PS (1999) The meta-analysis of response ratios in experimental ecology. Ecology 80:1150–1156. https://doi.org/10.1890/0012-9658(1999)080[1150:TMAORR]2.0.CO;2
IPCC (2021) Climate change 2021: the physical science basis. Contribution of Working Group I to the Sixth Assessment Report of the Intergovernmental Panel on Climate Change. Cambridge University Press Cambridge UK and New York NY USA. https://doi.org/10.1017/9781009157896

Islam MU, Ibrahim MM, Liu Y, Jiang F, Islam MM, Halder M, Hou E (2025) Phosphorus fertilization is essential for sustaining crop yields on converted natural ecosystems: a global meta-analysis. Soil Tillage Res 254:106756. https://doi.org/10.1016/j.still.2025.106756

Jiang Z, Vancov T, Fang Y, Tang C, Zhang W, Xiao M, Song X, Zhou J, Ge T, Cai Y, Yu B, White JC, Li Y (2025) Sustained superiority of biochar over straw for enhancing soil biological phosphorus via the mediation of *pho*D-harboring bacteria in subtropical Moso bamboo forests. For Ecol Manage 584:122606. https://doi.org/10.1016/j.foreco.2025.122606

Jiang Z, Tang C, Liu S, Fang Y, Zhou J, Xiao M, Luo Y, Ge T, Cai Y, Yu B, White JC, Li Y (2026a) Nano-zeolite-coupled biochar-based phosphate fertilizer suppresses the priming effect and promotes soil carbon stability in subtropical bamboo plantations. Ind Crops Prod 240:122720. https://doi.org/10.1016/j.indcrop.2026.122720

Jiang Z, Zhang S, Tang C, Xiao M, Zhou J, Luo Y, Ge T, Yu B, White JC, Li Y (2026b) Divergent effects of straw and biochar on soil carbon priming are depth-dependent in subtropical Moso bamboo forests. Biol Fertil Soils 62:349–365. https://doi.org/10.1007/s00374-025-01927-z

Joergensen RG (1996) The fumigation-extraction method to estimate soil microbial biomass: calibration of the k_{EC} value. Soil Biol Biochem 28:25–31. https://doi.org/10.1016/0038-0717(95)00102-6

Knorr W, Prentice IC, House JI, Holland EA (2005) Long-term sensitivity of soil carbon turnover to warming. Nature 433:298–301. https://doi.org/10.1038/nature03226

Li D, Schädel C, Haddix ML, Paul EA, Conant R, Li J, Zhou J, Luo Y (2013) Differential responses of soil organic carbon fractions to warming: results from an analysis with data assimilation. Soil Biol Biochem 67:24–30. https://doi.org/10.1016/j.soilbio.2013.07.008

Li Y, Li Y, Chang SX, Xu Q, Guo Z, Gao Q, Qin Z, Yang Y, Chen J, Liang X (2017) Bamboo invasion of broadleaf forests altered soil fungal community closely linked to changes in soil organic C chemical composition and mineral N production. Plant Soil 418:507–521. https://doi.org/10.1007/s11104-017-3313-y

Li J, Liu Z, Jin M, Zhang W, Lambers H, Hui D, Liang C, Zhang J, Wu D, Sardans J, Peñuelas J, Petticord D, Frey D, Zhu Y (2023) Microbial controls over soil priming effects under chronic nitrogen and phosphorus additions in subtropical forests. ISME J 17:2160–2168. https://doi.org/10.1038/s41396-023-01523-9

Li M, Zhao X, Cheng Y, Wu M, Dong C, Xiang H, Li Y, Cai Y, Zhuang Z, Yu B (2025) Zinc oxide nanoparticles coupled biochar-based slow-release fertilizer for enhanced nutrient efficiency and sustainable agriculture. Ind Crops Prod 232:121265. https://doi.org/10.1016/j.indcrop.2025.121265

Liang J, Li D, Shi Z, Tiedje JM, Zhou J, Schuur EAG, Konstantinidis KT, Luo Y (2015) Methods for estimating temperature sensitivity of soil organic matter based on incubation data: a comparative evaluation. Soil Biol Biochem 80:127–135. https://doi.org/10.1016/j.soilbio.2014.10.005

Liu X, Li Z, Reich PB, Zhou G, Yan J, Huang W, Wang Y, Peñuelas J, Tissue DT, Zhao M, Wu T, Wu D, Xu W, Li Y, Tang X, Zhou S, Meng Z, Liu S, Chu G, Zhang D, Zhang Q, He X, Liu J (2023) Long-term warming increased carbon sequestration capacity in a humid subtropical forest. Glob Chang Biol 30:e17072. https://doi.org/10.1111/gcb.17072

Liu Y, Wang H, Schindlbacher A, Liu S, Yang Y, Tian H, Chen L, Ming A, Wang J, Li J, Tian Z (2025) Soil respiration related to the molecular composition of soil organic matter in subtropical and temperate forests under soil warming. Soil Biol Biochem 201:109661. https://doi.org/10.1016/j.soilbio.2024.109661

Malik AA, Puissant J, Buckeridge KM, Goodall T, Jehmlich N, Chowdhury S, Gweon HS, Peyton JM, Mason KE, van Agtmaal M, Blaud A, Clark IM, Whitaker J, Pywell RF, Ostle N, Gleixner G, Griffiths RI (2018) Land use driven change in soil pH affects microbial carbon cycling processes. Nat Commun 9:3591. https://doi.org/10.1038/s41467-018-05980-1

Miranda-Trevino JC, Coles CA (2003) Kaolinite properties, structure and influence of metal retention on pH. Appl Clay Sci 23:133–139. https://doi.org/10.1016/S0169-1317(03)00095-4

Moinet GYK, Hunt JE, Kirschbaum MUF, Morcom CP, Midwood AJ, Millard P (2018) The temperature sensitivity of soil organic matter decomposition is constrained by microbial access to substrates. Soil Biol Biochem 116:333–339. https://doi.org/10.1016/j.soilbio.2017.10.031

Nottingham AT, Turner BL, Stott AW, Tanner EVJ (2015) Nitrogen and phosphorus constrain labile and stable carbon turnover in lowland tropical forest soils. Soil Biol Biochem 80:26–33. https://doi.org/10.1016/j.soilbio.2014.09.012

Qin S, Li C, Fang K, Zhang Q, Wang J, Liu F, Yu J, Yang Y (2019) Temperature sensitivity of SOM decomposition governed by aggregate protection and microbial communities. Sci Adv 5:aau1218. https://doi.org/10.1126/sciadv.aau1218

Raut SS, Sharma A, Mishra A (2025) Nano-bioremediation via biochar, zeolite nanocomposites for water quality enhancement: a review. Water Environ Res 97:e70151. https://doi.org/10.1002/wer.70151

Sáez-Sandino T, Maestre FT, Berdugo M, Gallardo A, Plaza C, García-Palacios P, Guirado E, Zhou G, Mueller CW, Tedersoo L, Crowther TW, Delgado-Baquerizo M (2024) Increasing numbers of global change stressors reduce soil carbon worldwide. Nat Clim Chang 14:740–745. https://doi.org/10.1038/s41558-024-02019-w

Shahjahan M, Iqbal Y, Javed S, Chatha SA, Tahir T, Shahzad K, Salman T, Qamar MA, Ullah S (2025) Zeolite-based biopolymer composites: innovations, applications, and future directions in biomedical engineering. Rev Inorg Chem. https://doi.org/10.1515/revic-2025-0081

Shi J, Gong J, Li X, Zhang Z, Zhang W, Li Y, Song L, Zhang S, Dong J, Baoyin TT (2023) Phosphorus application promoted the sequestration of orthophosphate within soil microorganisms and regulated the soil solution P supply in a temperate grassland in northern China: a ^{31}P NMR study. Soil Tillage Res 227:105612. https://doi.org/10.1016/j.still.2022.105612

Solangi F, Zhu X, Khan S, Rais N, Majeed A, Sabir MA, Iqbal R, Ali S, Hafeez A, Ali B, Ercisli S, Kayabasi ET (2023) The global dilemma of soil legacy phosphorus and its improvement strategies under recent changes in agro-ecosystem sustainability. ACS Omega 8:23271–23282. https://doi.org/10.1021/acsomega.3c00823

Song X, Peng C, Zhou G, Jiang H, Wang W, Xiang W (2013) Climate warming-induced upward shift of Moso bamboo population on Tianmu Mountain China. J Mt Sci 10:363–369. https://doi.org/10.1007/s11629-013-2565-0

Song X, Peng C, Zhou G, Gu H, Li Q, Zhang C (2017) Dynamic allocation and transfer of non-structural carbohydrates, a possible mechanism for the explosive growth of Moso bamboo (*Phyllostachys heterocycla*). Sci Rep 6:25908. https://doi.org/10.1038/srep25908

Song Y, Lin W, Gustave W, Zhang Y, Feng D, Zhang X, He F (2026) The promises and risks of carbon-based nanomaterials: a critical review on their roles in soil health and ecosystem safety. Environ Geochem Health 48:176. https://doi.org/10.1007/s10653-026-03068-0

Sun Q, Wang R, Wang Y, Du L, Zhao M, Gao X, Hu Y, Guo S (2018) Temperature sensitivity of soil respiration to nitrogen and phosphorus fertilization: does soil initial fertility matter? Geoderma 325:172–182. https://doi.org/10.1016/j.geoderma.2019.07.019

Tabatabai MA, Bremner JM (1969) Use of p-nitrophenyl phosphate for assay of soil phosphatase activity. Soil Biol Biochem 1:301–307. https://doi.org/10.1016/0038-0717(69)90012-1

Vance ED, Brookes PC, Jenkinson DS (1987) An extraction method for measuring soil microbial biomass C. Soil Biol Biochem 19:703–707. https://doi.org/10.1016/0038-0717(87)90052-6

von Lützow M, Kögel-Knabner I, Ekschmitt K, Flessa H, Guggenberger G, Matzner E, Marschner B (2007) SOM fractionation methods: relevance to functional pools and to stabilization mechanisms. Soil Biol Biochem 39:2183–2207. https://doi.org/10.1016/j.soilbio.2007.03.007

Whalen ED, Grandy AS, Geyer KM, Morrison EW, Frey SD (2024) Microbial trait multifunctionality drives soil organic matter formation potential. Nat Commun 15:10209. https://doi.org/10.1038/s41467-024-53947-2

Wu M, Lu J, Zhang Y, Ling Z, Lu R, Zhu J, Li Y, Cai Y, Xiang H, Zhang Z, Yu B (2025) Chitosan hydrogel membrane embedded by metal-modified biochars for slow-release fertilizers. Int J Biol Macromol 306:141296. https://doi.org/10.1016/j.ijbiomac.2025.141296

Wu R, Zhang Z, Li G, Wang X, Fang Y, Kuyakov Y, Xu X, Chen J, Ge T, Zhu Z (2026) Frequency and C:N:P stoichiometry of organic inputs determines intensity of net C balance in paddy soils. Soil Biol Biochem 214:110051. https://doi.org/10.1016/j.soilbio.2025.110051

Xiao M, Tang C, Jiang Z, Zhou J, Luo Y, Ge T, Pan L, Yu B, Cai Y, White JC, Li Y (2026) Opposing effects of maize straw and its biochar on soil N_2O emissions by mediating microbial nitrification and denitrification in a subtropical Moso bamboo forest. Biochar 8:50. https://doi.org/10.1007/s42773-025-00545-0

Yuan Y, Liang Y, Cai H, Yuan J, Li C, Liu H, Zhang C, Wang L, Zhang J (2025) Soil organic carbon accumulation mechanisms in soil amended with straw and biochar: entombing effect or biochemical protection? Biochar 7:33. https://doi.org/10.1007/s42773-024-00360-z

Zang H, Blagodatskaya E, Wen Y, Shi L, Cheng F, Chen H, Zhao B, Zhang F, Fan M, Kuzyakov Y (2020) Temperature sensitivity of soil organic matter mineralization decreases with long-term N fertilization: evidence from four Q_{10} estimation approaches. Land Degrad Dev 31:683–693. https://doi.org/10.1002/ldr.3496

Zhang L, Chang L, Liu H, Puy Alquiza MJ, Li Y (2025) Biochar application to soils can regulate soil phosphorus availability: a review. Biochar 7:13. https://doi.org/10.1007/s42773-024-00360-z

Zhou J, Tang C, Kuzyakov Y, Vancov T, Fang Y, Song X, Zhou X, Jiang Z, Ge T, Xu L, Cai Y, Yu B, White J, Gu B, Chen X, Ciais P, Li Y (2024) Biochar-based urea increases soil methane uptake in a subtropical forest. Geoderma 449:116994. https://doi.org/10.1016/j.geoderma.2023.116994

Zhou J, Delgado-Baquerizo M, Vancov T, Liu Y, Zhou X, Chen J, Fang Y, Liu S, Yu B, Zhou G, Gu B, White J, Chen X, Li Y (2026a) Biochar mitigates nitrogen deposition-induced enhancement of soil N_2O emissions in a subtropical forest. Biol Fertil Soils 62:291–305. https://doi.org/10.1007/s00374-025-01899-0

Zhou J, Tang C, Vancov T, Fu S, Fang Y, Ge T, Dong Y, Luo Y, Yu B, Cai Y, White J, Li Y (2026b) Biochar mitigates the suppressive effects of nitrogen deposition on soil methane uptake in a subtropical forest. Agric Ecosyst Environ 395:109951. https://doi.org/10.1016/j.agee.2024.109951

Zhu Z, Fang Y, Liang Y, Li Y, Liu S, Li Y, Li B, Gao W, Yuan H, Kuzyakov Y, Wu J, Richter A, Ge T (2022) Stoichiometric regulation of priming effects and soil carbon balance by microbial life strategies. Soil Biol Biochem 169:108669. https://doi.org/10.1016/j.soilbio.2022.108669